Talanta 128 (2014) 196–202

Contents lists available at ScienceDirect

Talanta

journal homepage: www.elsevier.com/locate/talanta

Gold nanorods for surface Plasmon resonance detection of mercury (II) in flow injection analysis

Khang Trieu [a], Emily C. Heider [a], Scott C. Brooks [b], Fernando Barbosa Jr.[c], Andres D. Campiglia [a,*]

[a] Department of Chemistry, University of Central Florida, P.O. Box 25000, Orlando, FL 32816-2366, USA
[b] Oak Ridge National Laboratory, Environmental Sciences Division, P.O. Box 2008, MS 6038, Oak Ridge, TN 37831-6038, USA
[c] Laboratório de Toxicologia e Essencialidade de Metais, Faculdade de Ciências Farmacêuticas de Ribeirão Preto, Universidade de São Paulo, Avenida do Café s/n, Monte Alegre, 1404903 Ribeirão Preto-SP, Brazil

ARTICLE INFO

Article history:
Received 19 March 2014
Received in revised form
16 April 2014
Accepted 17 April 2014
Available online 26 April 2014

Keywords:
Flow injection analysis
Localized surface Plasmon resonance
Gold nanorods
Mercury
Sensors

ABSTRACT

This article investigates the flow injection analysis of mercury (II) ions in tap water samples via surface Plasmon resonance detection. Quantitative analysis of mercury (II) is based on the chemical interaction of metallic mercury with gold nanorods immobilized on a glass substrate. A new flow cell design is presented with the ability to accommodate the detecting substrate in the sample compartment of commercial spectrometers. Two alternatives are here considered for mercury (II) detection, namely stop-flow and continuous flow injection analysis modes. The best limit of detection (2.4 ng mL^{-1}) was obtained with the continuous flow injection analysis approach. The accurate determination of mercury (II) ions in samples of unknown composition is demonstrated with a fortified tap water sample.

1. Introduction

Flow injection analysis (FIA) methods have been used extensively since the 1970s when they were first utilized to achieve automation of serial assays. In addition to quantitative analysis applications, FIA has been used to evaluate reaction rates, diffusion constants, and solubility products, among many other fundamental values [1,2]. Most FIA methods on mercury detection base quantification on peak height by the detection method of choice, most commonly spectrophotometric, luminescence, inductively-coupled plasma atomic emission and mass spectrometry, electrochemical, and enzymatic [3–7].

Our approach to mercury detection monitors wavelength shifts in the maximum absorption of gold nanorods (Au NRs) [8–10]. When Au NRs are exposed to the presence of Hg(0), the amalgamation between Au and Hg(0) causes a reduction of the effective aspect ratio (length/diameter) of the nanoparticles and a blue-shift of their longitudinal surface Plasmon resonance (LSPR) maximum absorption wavelength (λ_{max}). Quantitative analysis is made possible by the linear correlation that exists between the concentration of mercury in the water sample and the position of the LSPR λ_{max} of Au NRs [8–12].

Previous studies in our group were carried out under batch (static) conditions [8–10]. The analytical capabilities of Au NRs immobilized on a glass substrate were compared to solution measurements with colloidal NRs. Under batch conditions, the immobilization of Au NRs on a glass substrate improved both the sensitivity and the limits of detection of the sensing approach [9]. Herein, we extend our investigations to the analysis of Hg^{2+} in tap water flows. Immobilized NRs are compared to their colloidal counterparts for the analysis of water samples with high ionic strengths. The analytical figures of merit obtained with Au NRs glass substrates are evaluated via stop-flow and continuous-flow injection analysis modes. These two scenarios represent a range of experiments an analyst could face in any given analytical procedure, each giving rise to unique advantages and limitations for the analysis of mercury.

2. Experimental

2.1. Reagents and supplies

Bare Au NRs with aspect ratio 1.9, nominal LSPR λ_{max} of 611 nm and capped with cetyl trimethylammonium bromide (CTAB) were

* Corresponding author. Tel.: +1 407 823 4162; fax: +1 407 823 2252.
E-mail addresses: khangtrieu818@knights.ucf.edu (K. Trieu), Emily.Heider@ucf.edu (E.C. Heider), brookssc@ornl.gov (S.C. Brooks), fbarbosa@fcfrp.usp.br (F. Barbosa Jr.), andres.campiglia@ucf.edu (A.D. Campiglia).

http://dx.doi.org/10.1016/j.talanta.2014.04.028
0039-9140/

purchased from Nanopartz, Inc. (Loveland, CO). VWR Vistavision cover slides were purchased from VWR International (Radnor, PA) and cut to size. Reagents, including $HgCl_2$, NaCl, H_2SO_4, ethanol, $Al(NO_3)_3$, $Co(NO_3)_2$, $Cr(NO_3)_3$, $Sr(NO_3)_2$, $SnCl_2$, $Pb(NO_3)_2$, Mn $(CH_3COO)_2$, $MgSO_4$, H_2O_2 (30%), $NaBH_4$, and 85% (3-mercapto-propyl)trimethoxysilane (MPTMS) were acquired from Fisher Scientific. Otherwise noted, all solutions were prepared using 18 MΩ cm Nanopure water. Glass slides were purchased from VWR International.

2.2. Immobilization of Au NR on a glass substrate

Au NRs were immobilized on glass substrates according to a procedure slightly modified since our last report [9]. Glass cover slides were cleaned by immersing them into a piranha solution – a 4:1 concentrated sulfuric acid to 30% hydrogen peroxide mixture – for 20 min. After rinsing with copious quantities of water and methanol, the clean substrates were storage in methanol. A thiol-functionalized, self-assembled monolayer was deposited on the glass surface by immersing the clean slides into a MPTMS/ethanol mixture (10/90 v/v) for 1 h. The MPTMS functionalized substrates were rinsed copiously with methanol and then oven-heated to 110 °C for 3 h.

With the aim of minimizing the electrostatic repulsion among Au NRs and achieve a better surface coverage on the MPTMS substrates, the commercial solution of Au NRs was stripped from the excess of CTAB [13]. This was accomplished by centrifuging 1 mL of Au NRs solution (2.23×10^{11} NRs/mL) at 2033*g* for 30 min. After removing approximately 800 μL of the supernatant from the sample vial, the Au NRs were re-suspended in approximately the same volume of Nanopure water. This process was repeated twice. Additional rounds of centrifugation resulted in irreversible aggregation of Au NRs.

The nanoparticles were immobilized on the MPTMS substrates by placing 500 μL of Au NRs solution on the functionalized surface and let it sit for four hours. After removing the excess of unreacted NRs with water, the Au NRs substrates were stocked in Nanopure water until further use. Their absorption properties were found to remain constant within a six-month period of substrate preparation. Longer time periods were not attempted.

2.3. Instrumentation

Flow injection analysis was carried out with a FIA-lab system (FIAlab – 2000, Alitea Instruments USA, Inc.) operating in the single-line manifold configuration. The main components of the FIA-lab system consisted of a four channel peristaltic pump equipped with 0.75 mm internal diameter (i.d.) Teflon tubing, a sample injection valve, a T-piece, and a reaction coil (0.75 mm i.d. and 195 cm long). From the reaction coil, the sample was pumped to the flow- through detection cell and then to waste. For all experiments the sample loop injection volume was 150 μL.

Fig. 1 shows a schematic diagram of the demountable flow cell used to measure absorbance spectra from Au NRs immobilized on solid substrates. The basic unit (SL-5 EZ) was purchased from International Crystal Laboratories (Garfield, NJ) and modified in-house to fit Au NRs substrates. A silicon gasket was cut to the dimensions of the cell providing an inner cell volume equal to 15 μL.

Absorbance measurements were made with a double-beam Cary 50 spectrometer equipped with a 75-W pulsed Xenon lamp (spectral radiance from 190 to 1100 nm), a 1.5-nm fixed optical band-pass, a monochromator with a 24,000 nm/min maximum scan rate, a beam-splitter and two silicon photodiode detectors.

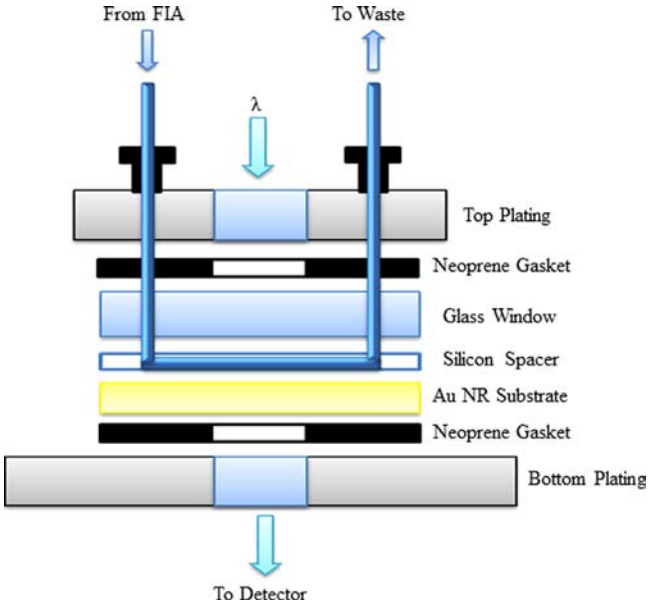

Fig. 1. Schematic diagram of the flow cell used to measure absorbance from Au NRs substrates. The sample flow is indicated by the solid blue line that is exposed to the Au NRs substrate (yellow). Excitation radiation from the spectrometer passes through the flow cell via glass windows (light blue), allowing to record spectra during the flow of sample. (For interpretation of the references to color in this figure legend, the reader is referred to the web version of this article.)

2.4. Software

Nonlinear peak fitting of spectral data was made with OriginLab 8.5 software.

3. Results and discussion

3.1. Instrumental performance and spectral fitting for accurate assignment of maximum absorption wavelengths

Quantitative analysis with the proposed sensor is based on maximum absorption spectral shifts ($\Delta\lambda_{max}$) upon mercury interaction with Au NRs. In the ideal case scenario – i.e., the absence of environmental noise – the ability to measuring reproducible wavelengths ultimately depends on the performance of the spectrometer. Table 1 summarizes the typical reproducibility of wavelength measurements of the spectrometer used in these studies. Instrumental performance was monitored daily with a commercial standard from Photon Technology International. The standard consisted of a single crystal of dysprosium-activated yttrium aluminum garnet mounted in a cuvette-sized holder with a well-characterized, quasi-line absorption spectrum in the visible region. Wavelength accuracy was monitored by comparing the position of several atomic lines obtained with the spectrometer to the maximum wavelengths provided by the manufacturer. The reported averages and standard deviations in Table 1 represent 10 measurements made within 1 h of instrumental use. The performance of the spectrometer was confirmed on different days and for longer periods of instrumental use.

The extent to which instrumental noise deteriorates the accurate assignment of λ_{max} depends on the signal intensity of absorption spectra. The magnitude of the absorbance intensity is directly proportional to the amount of Au NRs either in solution or immobilized on a glass substrate. Although it is always possible to adjust the concentration of Au NRs to improve the signal-to-noise ratio, the larger wavelength shifts per unit concentration of

Table 1
Reproducibility of measurements[a] obtained with UV–vis absorption spectrometer.

λ (nm)	385.70 ± 0.07	395.08 ± 0.07	447.27 ± 0.07	456.24 ± 0.07	751.88 ± 0.07	754.22 ± 0.07	761.42 ± 0.07	789.16 ± 0.07
I (r.u.)	0.1858 ± 0.0012	0.1410 ± 0.0018	0.1303 ± 0.0007	0.1039 ± 0.0010	0.1433 ± 0.0011	0.1358 ± 0.0026	0.1043 ± 0.0019	0.1084 ± 0.0029

[a] Reported averages are based on 10 scans recorded within one hour of instrumental use. Wavelength (λ) and intensity (I) measurements were made from a commercial standard consisting of a single crystal of dysprosium-activated yttrium aluminum garnet mounted in a cuvette size holder.

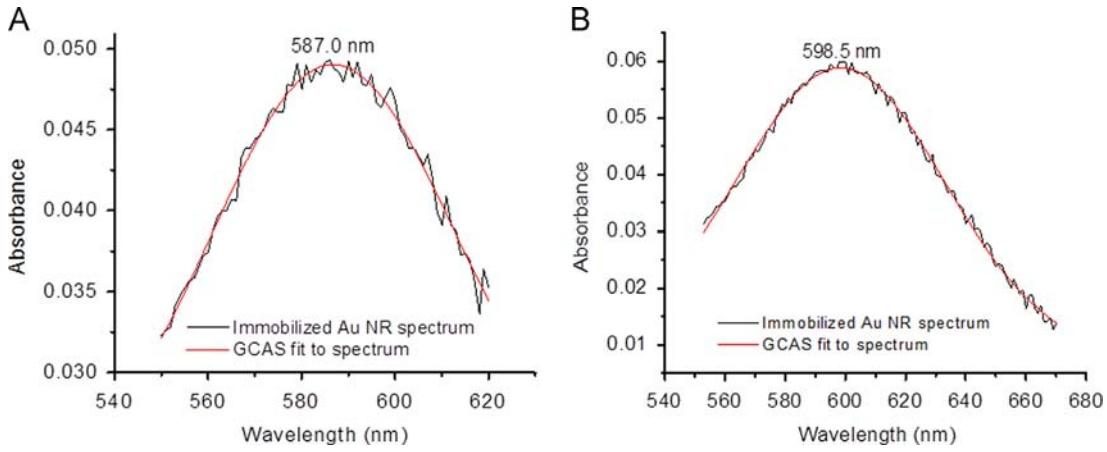

Fig. 2. Absorbance spectrum of Au NR substrate with curve fitting using the Gram-Charlier (GCAS) function (χ^2 tolerance of 1×10^{-9}). Spectra were recorded from glass substrates with different number of Au NRs on their surface: (A) 1.8×10^{11} and (B) 2.2×10^{11} NRs. Number of Au NRs was estimated according to Ref. [9].

mercury are obtained with relatively low concentrations of Au NRs [8–10,14].

Under this prospective, the accurate analysis of trace concentrations of mercury is related to the ability of assigning accurate λ_{max} from noisy absorption spectra. One possible way to facilitate accurate λ_{max} assignments is the nonlinear fitting of noisy spectral data to a Gram-Charlier (GCAS) function using a Levenberg Marquardt iteration algorithm. [15] Examples of absorbance spectra and their corresponding GCAS fits are shown in Fig. 2. This approach was used to calculate all the $\Delta\lambda_{max}$ values used in this study. A tolerance (χ^2) of 1×10^{-9} was employed in all cases.

3.2. Stabilization of reference wavelength with $NaBH_4$

In order to obtain a stable λ_{max} for reference purposes, the treatment of NRs substrates with $NaBH_4$ is necessary previous to mercury detection. Fig. 3 illustrates the typical behavior of absorbance spectra recorded from Au NRs substrates immersed in 10^{-3} M $NaBH_4$. Similar behaviors were observed with 10^{-2} and 0.1 M $NaBH_4$. The blue-shift of the λ_{max} results from unreacted gold ions (Au^{3+}) still present on the glass surface of the substrate. Their reduction to Au (0) and subsequent deposition on the immobilized NRs removes CTAB molecules from the surface of the nanoparticles, increases the diameter of the NRs and reduces their aspect ratio [8–10]. Since the λ_{max} stops shifting at approximately 6 min of $NaBH_4$ exposure time, all further measurements were made with NRs substrates previously exposed to 10 min of $NaBH_4$. Under these conditions, the statistics of the fittings of numerous absorption spectra recorded from individual substrates provided a ± 1 nm substrate-to-substrate variation of the average λ_{max} value.

3.2.1. Effect of ionic strength on the spectral features of colloidal and immobilized Au NRs

A considerable number of tap water samples tested in our lab changed the spectral properties of colloidal NRs. An example of the observed modifications is shown in Fig. 4A, which compares

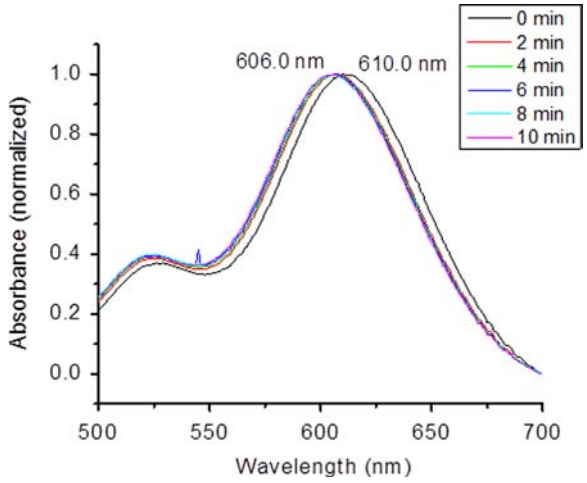

Fig. 3. Absorbance spectra over time of Au NR substrate immersed in a 10^{-3} M $NaBH_4$/Nanopure water solution. The 0 min spectrum was recorded before adding the reducing agent to the aqueous solution with the Au NR substrate.

absorbance spectra recorded from colloidal NRs exposed to a tap water sample in the presence of 0.01 M $NaBH_4$. The decrease in signal intensity and the broadening of the LSPR absorbance peak can be attributed to the aggregation of Au NRs, a phenomenon that usually occurs in aqueous solutions with relatively high ionic strengths. [13] The main reason for the aggregation of NRs in high ionic strength media is the deterioration of the CTAB bilayer and its electrostatic shielding effect, which ultimately results in the reduction of inter-nanoparticle repulsive forces.

Fig. 4B compares the absorption spectra of colloidal NRs exposed to a Nanopure water sample with increasing ionic strength. The ionic strength of the water samples was adjusted with NaCl concentrations varying from 0 to 100 μM. All water samples contained 0.01 M $NaBH_4$ and all spectra were recorded after 10 min of exposure time. To some extent, the spectral

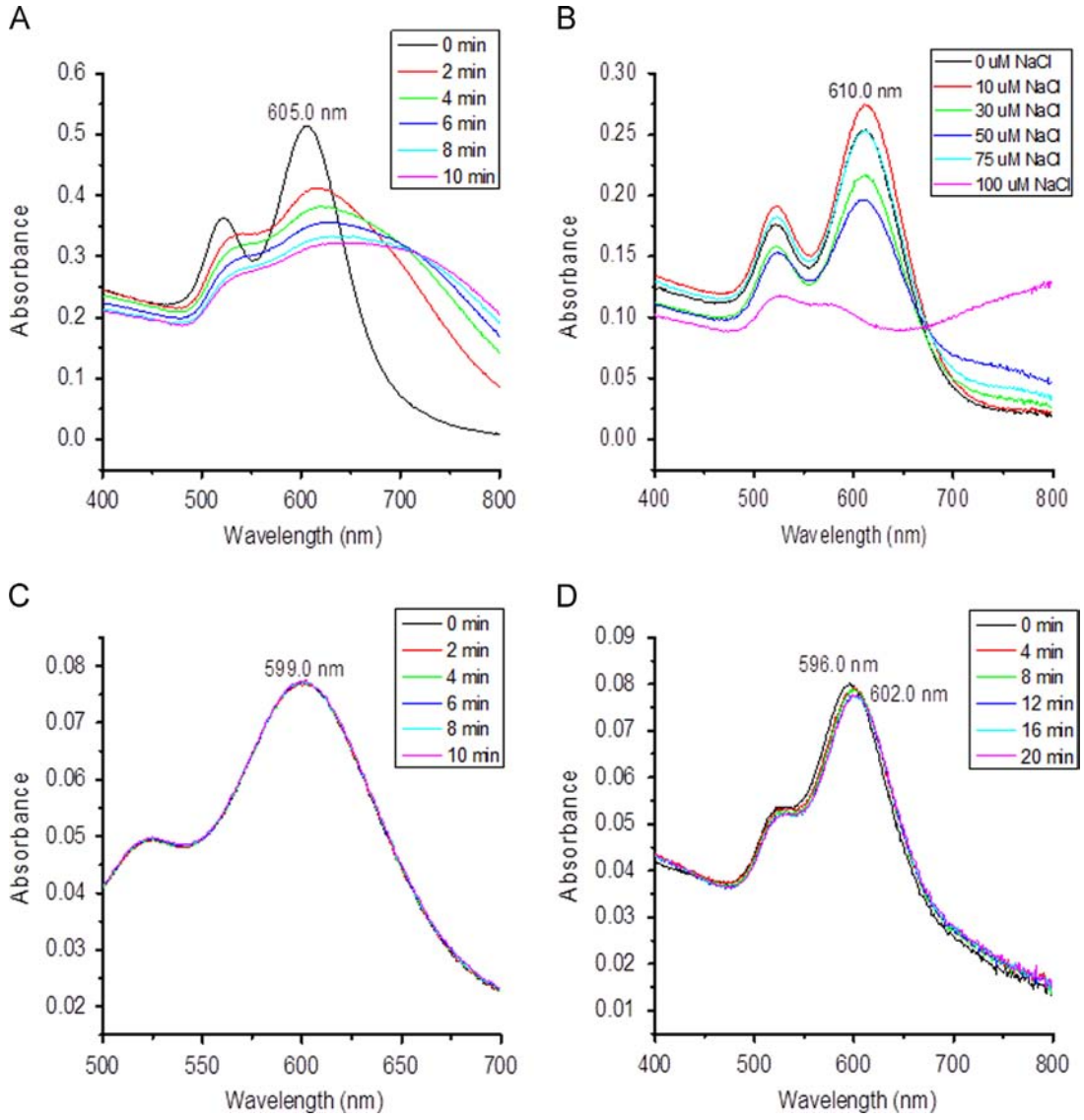

Fig. 4. Absorbance spectra of colloidal NRs recorded (A) as a function of time exposure to a tap water sample in 0.01 M $NaBH_4$ and (B) after 10 min of time exposure to various concentrations of NaCl in 0.01 M $NaBH_4$/Nanopure water. Absorbance spectra of immobilized NRs recorded as a function of time exposure to (C) a 0.5 M NaCl in 0.01 M $NaBH_4$/Nanopure water and (D) a tap water sample and 0.01 M $NaBH_4$.

changes in 100 μM NaCl are similar to those observed after 2 min of tap water exposure.

The same is not true for Au NRs immobilized on a glass substrate (see Fig. 4C). Immobilization on the glass substrate probably prevents aggregation of Au NRs by limiting their physical movement. As shown in Fig. 4D, relatively stable absorbance spectra were also observed from NRs substrates exposed to tap water samples. Although a small red-shift of the λ_{max} was initially observed, its stabilization after approximately 10 min of exposure time provided a reproducible reference wavelength ($\lambda_{max} \pm 1$ nm) for sensing mercury in tap water flows.

3.3. Analytical figures of merit (AFOM)

Two detection modes – stop and continuous flow – were investigated for the analysis of mercury in water samples. Stop-flow experiments were carried out by pumping Nanopure water through the flow cell at a 0.73 mL min^{-1} rate. Standard solutions of Hg^{2+} were prepared in 0.01 M $NaBH_4$. After 30 s of sample injection, the carrier flow was stopped to allow for the interaction of the injected solution with the NRs substrate. The 30 s period was the time we observed to elapse between the injection of a color dye solution and its arrival at the sensing cavity of the flow cell. Within the micro-molar Hg (II) concentration range, reaction completion between Hg (0) and Au NRs occurred at approximately three minutes of substrate exposure time (see Fig. 5A). All wavelength shifts, therefore, were then measured after 5 min of equilibration time. Continuous-flow experiments were carried out by pumping standard solutions of $Hg^{2+}/10^{-3}$ M $NaBH_4$ at a 0.73 mL min^{-1} flow rate. All wavelength shifts were measured after 10 min of sample flow, a time period long enough to reach maximum and constant wavelength shifts within the nano-molar Hg (II) concentration range (see Fig. 5B and C).

Table 2 summarizes the AFOM obtained with the two approaches. The linear dynamic ranges (LDR) of the calibration curves were based on five Hg (II) concentrations. The entire set of stop-flow data was obtained with one NRs substrate. Including the one substrate for blank measurements (10^{-3} M $NaBH_4$/Nanopure water), generating the entire set of continuous-flow data required the use of six NRs substrates. The correlation coefficients obtained from the least squares fitting ($\Delta\lambda_{max} = b \cdot [Hg^{2+}] + a$) [16] close to unity demonstrate the existence of a linear relationship between

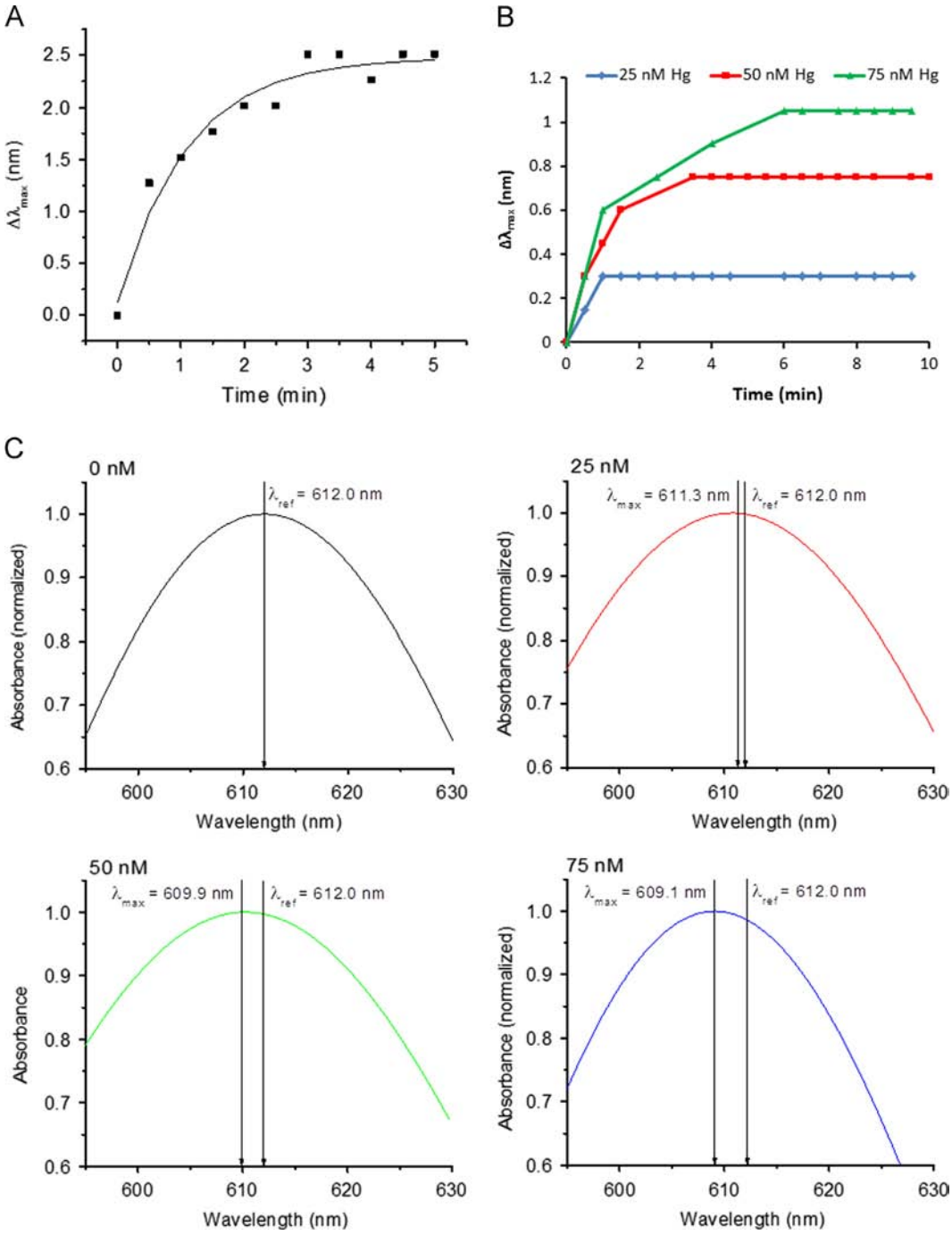

Fig. 5. Shift of the SPR maximum wavelength of Au NRs substrates ($\Delta\lambda_{max}$) recorded as a function of time exposure to (A) 2 μM concentration of Hg (II) in 0.01 M $NaBH_4$/Nanopure water. (B) nano-molar concentrations of Hg (II) in 10^{-3} M $NaBH_4$/Nanopure water. Wavelength shifts were recorded under (A) stop-flow conditions with one Au NRs substrate; and (B) continuous flow conditions using one Au NRs substrate per Hg (II) concentration. (C) Normalized GCAS fitted absorbance spectra of Au NR substrates showing maximum wavelength shift after 10 min exposure to nM mercury concentrations. Reference SPR wavelength (0 nM)=612.0 nm.

$\Delta\lambda_{max}$ and Hg (II) concentration. The limits of detection (LODs) were calculated as $3\times s_a/b$; where s_a is the standard deviation of the intercept ($\Delta\lambda_{max}=a\pm s_a$) when [$Hg^{2+}$]=zero and b is the slope (calibration sensitivity) of the linear plot. The limits of quantitation (LOQ) were calculated as $10\times s_a/b$. Comparison of their values shows a $LOQ_{continuous\text{-}flow}$ approximately 30× better than the $LOQ_{stop\text{-}flow}$. The better LOQ result from the steeper slope of the continuous-flow calibration curve ($b_{continuous\text{-}flow}=10.9\times b_{stop\text{-}flow}$) and the lower standard deviation of the intercept ($s_{a\ stop\text{-}flow}=2.9\times s_{a\ continuous\text{-}flow}$). The LOD obtained via the continuous-flow approach (11.7 nM) is of the same order of magnitude of the maximum contamination level (MCL=2 ng $ml^{-1}\equiv 9.97$ nM) set for mercury by the EPA in drinking water samples. [17]

3.4. Analysis of tap water samples

It is well known that Hg (0) forms amalgams with several metals [18]. Four methods have been reported for the different types of Hg amalgams known so far, namely: (1) direct physical contact with the other metal in the presence of a dilute acid; (2) immersion of the other metal in a liquid solution of a mercury salt; (3) immersion of Hg (0) in a liquid solution of a salt of the

Table 2
Analytical figures of merit for Hg (II) detection via the stop flow or continuous flow injection analysis method.

	Stop flow method	Continuous flow method
Linear dynamic range[a]	1.21–5.00 × 0^{-6} M	3.93–7.5 × 10^{-8} M
Linear Fitting[b]	$\Delta\lambda_{max}=(3.6\times10^{6})\cdot[Hg]+0.3$	$\Delta\lambda_{max}=(4.0\times10^{7})\cdot[Hg]-0.1$
Standard deviation of the intercept[c]	± 0.4 nm	± 0.2 nm
Standard deviation of the slope[c]	± 0.1 × 10^{6} nm M^{-1}	± 0.3 × 10^{7} nm M^{-1}
Calibration sensitivity	3.6 × 10^{6} nm M^{-1}	4.0 × 10^{7} nm M^{-1}
Correlation coefficient	0.9969	0.9861
Limit of detection	3.64 × 10^{-7} M	1.18 × 10^{-8} M
Limit of quantitation	1.21 × 10^{-6} M	3.93 × 10^{-8} M

[a] Linear dynamic range = Limit of quantitation − upper limit of detection.
[b] Equation for the best linear fit: $\Delta\lambda_{max}=b\cdot[Hg]+a$ where b = calibration sensitivity and a = intercept.
[c] Calculated according to Ref. [13].

Table 3
Elements capable of forming amalgams with Hg (0)[a].

Method[b]	Elements
1	Sb, As, Bi, Cd, Au, Pb, Mg, K, Ag, Na, Te, Th, Sn and Zn
2	Cu, Au, Pt, Ag and Pd
3	Zn and Na
4	All of the above

[a] According to Ref. [16] and [17].
[b] See text for method details.

Table 4
Chemical species tested for interference.

Contaminant	Chemical Form	MCL[a]
Manganese	$Mn(C_2H_3O_2)_2$	0.05 mg/L (0.91 μM)
Magnesium[b]	$MgSO_4$	
Cadmium	$Cd(NO_3)_2$	0.005 mg/L (0.04 μM)
Tin[b]	$SnCl_2$	
Lead	$Pb(NO_3)_2$	0.015 mg/L (0.07 μM)
Strontium[b]	$Sr(NO_3)_2$	
Aluminum	$Al(NO_3)_3$	0.2 mg/L (7.41 μM)
Chromium	$Cr(NO_3)_3$	0.1 mg/L (1.92 μM)
Cobalt[b]	$Co(NO_3)_2$	

[a] EPA- MCL in fresh water samples. See Ref. [14].
[b] No EPA-MCL value was found. See Ref. [14].

other metal; and (4) amalgamation via electrolysis. Table 3 groups the elements capable of forming metallic amalgams with Hg (0) via each method. The kinetics of amalgamation depends on the experimental conditions upon which the contact with the other metal occurs. Within the time-frame of our experiments (minutes) and the experimental conditions of our measurements, the only metal that forms an amalgam with Hg (0) is Au [19]. Metals such as lead, tin and zinc typically require an excess of Hg (0) (> 70 wt% Hg (0)) as well as high temperatures (≈ 500 K) and pressures (≈ 70 psi). Therefore, the amalgamation of Hg (0) with other metals in water samples under usual sensing conditions is negligible and it should not interfere with the accuracy of measurements.

Table 4 presents a list of inorganic ions commonly found in fresh water samples [20] tested in our lab for potential interference due to their interaction with the Au NRs on the glass substrate. Each ion was tested at the 5.0 μM concentration. Fig. 6A plots the total shift of the λ_{max} observed after the sequential injection of each inorganic salt into the FIA system. Each wavelength shift was measured in the stop flow mode after 5 min of inorganic salt injection. All measurements were made with the same substrate in the presence of 10^{-3} M $NaBH_4$/Nanopure water. After measuring the wavelength shift caused by each inorganic salt, the cell was flushed for 5 min with 10^{-3} M $NaBH_4$/Nanopure water at a 0.73 mL min^{-1} flow rate. Clearly, the successive addition of inorganic ions to the flow cell causes a considerable λ_{max} shift that could affect the accuracy of analysis. The plateau that was reached after the addition of $Cr(NO_3)_3$ is probably due to the surface saturation of Au NRs and the lack of available sites for further interactions with Co^{2+} ions. This assumption is supported by the wavelengths shift we observed from a second substrate individually probed with 5 μM $Co(NO_3)_2$.

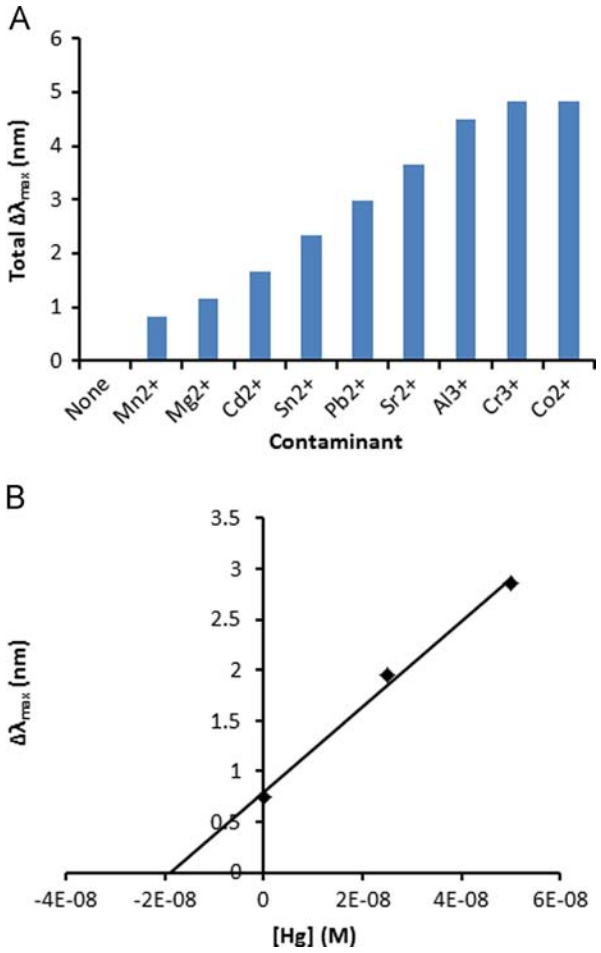

Fig. 6. Shift of the SPR maximum wavelength of Au NRs substrates ($\Delta\lambda_{max}$) recorded: (A) after 5 min of successive exposure to 5.0 μM concentrations of each inorganic salt in 10^{-3} M $NaBH_4$/Nanopure water and (B) as a function of multiple standard additions of Hg (II) to a fortified tap water sample in the presence of 10^{-3} M $NaBH_4$. Wavelength shifts were recorded under (A) stop-flow conditions with one Au NRs substrate and (B) continuous flow conditions using one Au NRs substrate per Hg (II) concentration.

One possibility to account for the contribution of concomitant ions to the total wavelength shift is to measure the blank signal of a synthetic mixture tailored to mimic the typical composition of inorganic ions in fresh water samples [20]. The feasibility of this approach was tested in our lab with a tap water sample of unknown composition. Analysis was made under the continuous-flow mode via the calibration curve method. The λ_{max} of a NRs substrate was monitored for 10 min under the flow of tap water (0.73 mL min^{-1}) in the presence of 10^{-3} M $NaBH_4$. Since no change in the reference wavelength was observed, the tap water sample was fortified with $HgCl_2$ to provide a final standard Hg^{2+} concentration (18 nM) above the LOD of the method (11.7 nM). After placing a new substrate in the flow cell and flowing the sample for 10 min at the same rate (0.73 mL min^{-1}), a $[Hg^{2+}]=20.5$ nM was obtained.

The somehow high relative error ($E_r=100 \cdot [(20.5\ nM-18\ nM)/18\ nM]=13.9\%$) made us suspicious of the presence of unaccounted matrix interference. A multiple standard additions experiment was then undertaken to account for the potential interference of the unknown matrix. Fig. 6B shows the multiple standard addition plot of the tap water sample under continuous flow conditions. One substrate was used to generate the entire data set. The blank signal was estimated from the same standard mixture of inorganic ions used in the calibration curve procedure. The least-squares fitting of the experimental data displays a linear correlation ($R=0.9966$) for the equation $\Delta\lambda_{max}=0.042[Hg^{2+}]=0.802$. Extrapolation of the linear fitting to $\Delta\lambda_{max}=$zero yielded a $[Hg^{2+}]=19.1$ nM. This concentration presents a considerably lower relative error ($E_r=6.1\%$) than the one previously obtained by the calibration curve method.

4. Conclusions

The immobilization of Au NRs on glass substrates expands the applications of the mercury sensor to the FIA of water. In comparison to their colloidal counterparts, immobilized NRs showed better capability to analyze water samples with relatively high ionic strengths. By restricting their physical movement on the glass substrate, the immobilization of NRs prevents their aggregation in aqueous media, preserves their spectral features and provides a stable absorption spectrum for sensing purposes. The synthetic procedure for Au NRs immobilization provided glass substrates with $a\pm1$ nm λ_{max} variation. Since all $\Delta\lambda_{max}$ were calculated by using the λ_{max} of each substrate as the reference wavelength, it is safe to state that the ±1 nm substrate-to-substrate variation did not interfere significantly with the accuracy of the sensor.

The best LOD (11.7 nM=2.4 ng mL^{-1}) was obtained with the continuous flow method, which is of the same order of magnitude as the MCL (2 ng mL^{-1}) stipulated by the EPA for drinking waters [17]. With the current flow cell, an LOD improvement should be possible by increasing the volume of water flowed through the cell. The sample volume can be easily increased by using a faster flow rate, longer sample flowing times or both. This is a considerable advantage of the continuous flow method over the stop flow method. LOD improvements via the stop flow method require a new cell design that optimizes the interaction of Au NRs with the small sample volumes injected in the FIA system. The sensitive detection of mercury via the stop flow method should prove useful in cases of limited availability of samples.

Independent of the detection mode, the accurate determination of Hg (II) with the proposed sensor requires compensating for the interaction of concomitant ions with the NRs substrate. In the case of tap water samples, accuracy of analysis was accomplished by measuring the blank signal of a synthetic mixture tailored to mimic the typical composition of inorganic ions in fresh water samples.

Acknowledgments

This work was funded by U.S. Department of Energy (DE-SC0004813).

References

[1] J. Růžička, E.H. Hansen, Flow Injection Analysis, Wiley-Interscience, New York, 1988.
[2] M. Valcarcel, M.D. Luque de Castro, Flow-Injection Analysis Principles and Applications, Ellis Horwood Limited, Chichester, England, 1987.
[3] S. Pirvutoiu, I. Surugiu, E.S. Dey, A. Ciucu, V. Magearu, B. Danielsson, Analyst 126 (2001) 1612–1616.
[4] G. Tao, S.N. Willie, R.E. Sturgeon, Analyst 123 (1998) 1215–1218.
[5] E.M. Richter, M.A. Augelli, G.H. Kume, R.N. Mioshi, L. Angnes, Fresenius' J. Anal. Chem. 366 (2000) 444–448.
[6] L.A.d. Paz, A. Alegría, R. Barberá, R. Farré, M.J. Lagarda, Food Chem. 58 (1996) 169–172.
[7] C.P. Hanna, J.F. Tyson, Ana. Chem. 65 (1993) 653–656.
[8] M. Rex, F.E. Hernandez, A.D. Campiglia, Anal. Chem. 78 (2006) 445–451.
[9] E.C. Heider, K. Trieu, A.F.T. Moore, A.D. Campiglia, Talanta 99 (2012) 180–185.
[10] E.C. Heider, K. Trieu, V.M. Diaz, K.Y. Chumbimuni-Torres, A.D. Campiglia, S. J. Duranceau, Microchim. Acta 180 (2013) 1013–1020.
[11] H. Huang, C. Qu, X. Liu, S. Huang, Z. Xu, Y. Zhu, P.K. Chu, Chem. Commun. 47 (2011) 6897–6899.
[12] D. Li, G. Zheng, X. Ding, J. Wang, J. Liu, L. Kong, Colloids Surf. B: Biointerfaces 110 (2013) 485–488.
[13] A.R. Ferhan, L. Guo, D.H. Kim, Langmuir 26 (2010) 12433–12442.
[14] J. Perez-Juste, I. Pastoriza-Santos, L. Liz-Marzan, P. Mulvaney, Coord. Chem. Rev. 249 (2005) 1870–1901.
[15] A. Davis, in: S. Kotz, C.B. Read, N. Balakrishnan, B. Vidakovic (Eds.), Encylopedia of Statistical Sciences, John Wiley, New York, 1983, pp. 474–477.
[16] K. Danzer, L.A. Currie, Pure Appl. Chem. 70 (1998) 993–1014.
[17] ⟨http://www.epa.gov/safewater/consumer/pdf/mcl.pdf⟩ (accessed: 20.2.14).
[18] F. Habashi, Gordon and Breach Science (1989).
[19] P. Zaleski-Ejgierd, P. Pyykko, J. Phys. Chem. A 113 (45) (2009) 12380–12385.
[20] ⟨https://www-s.nist.gov/srmors/certificates/view_certPDF.cfm?certificate=1640a⟩ (accessed 10.03.14).